Ceramics-Silikáty 66 (4), 462-470 (2022)
www.ceramics-silikaty.cz doi: 10.13168/cs.2022.0042

EFFECT OF $MgO/MgSO_4$ MOLAR RATIO ON THE HYDRATION AND MECHANICAL PROPERTIES OF BMS CONTAINING STEEL SLAG

XUAN HE*, #HUANG LEI*,**, JIANG TAO***,****, CHENGYOU WU*,**

*Department of Civil Engineering, Qinghai University, Xining 810016, China
** Qinghai Provincial Key Laboratory of Energy-saving Building Materials and Engineering Safety, Xining 810016, China
***Qinghai Building and Materials Research Co., Ltd, Xining 810016, China
****Qinghai Provincial Key Laboratory of Plateau Green Building and Eco-community, Xining 810016, China

#E-mail: leihyx@foxmail.com

Submitted July 25, 2022; accepted September 14, 2022

Keywords: Basic magnesium sulfate cement, Steel slag, Hydration process, Compressive strength, Pore structures

The work aims to investigate the effect of $MgO/MgSO_4$ molar ratio (MSMR) on the hydration and mechanical properties of basic magnesium sulfate (BMS) cement and basic magnesium sulfate with the incorporation of steel slag (BMS-SS). The exothermic rate and cumulative heat release were monitored, and the hydration products and pore structures were analysed. In addition, the compressive strength was measured. The results show that the hydration process of BMS and BMS-SS are both affected by the MSMR; samples with an MSMR of 7 have the highest cumulative heat both for the BMS and BMS-SS. A higher MSMR has a negative effect on the formation of 5-1-7 and leads to the formation of $Mg(OH)_2$. The incorporation of SS leads to the formation of gypsum, especially for the samples with a low MSMR. Both the porosity and its distribution are affected by the MSMR, the porosity of the samples with an MSMR of 5 are significantly higher than those with an MSMR of 7 and 9, and the average pore diameter of the sample with an MSMR of 7 is the lowest whether or not SS is incorporated. The compressive strength of the samples with an MSMR of 7 and 9 are nearly equal and prominently higher than the samples with an MSMR of 5. The SS incorporation leads to a decrease in the compressive strength for all the samples.

INTRODUCTION

As a kind of low-carbon, energy-efficient, and environmentally friendly cementitious material, magnesium-based cement has developed rapidly in recent years [1-3]. The main common magnesium-based cements include magnesium chloride cement (MOC), sulfur magnesium oxychloride cement (MOS), and magnesium phosphate cement (MPC). Although these cements have many advantages, there are some drawbacks that are not conducive to the promotion and utilisation of magnesium-based cements. Many researchers have devoted their efforts to improving and optimising the characteristics.

Wu made significant progress in the modification of the characteristics of MOS by adding certain admixtures [4]. The author named the cement as Basic Magnesium Sulfate Cement (BMS). A new kind of hydration product $5Mg(OH)_2$-$MgSO_4$-$7H_2O$ (5-1-7) was found [5], which sustains the excellent performance of BMS, including the early strength, high strength, water, and corrosion resistance [6, 7].

In an attempt to further improve the properties of BMS, Wu et al. [8], Wang et al. [9, 10], Tan et al.[11] and Guo et al. [12] investigated the effects of some chemical admixtures, such as tartaric acid, phosphate, citric acid, amino trimethylene phosphonic acid, and sodium malate, on the basic mechanical properties, water resistance, and shrinkage deformation of BMS. The results showed that these chemical additives could effectively promote the formation of 5-1-7, increase the compactness of the microstructure and improve the compressive strength and water resistance of BMS. Indeed, others have investigated the addition of mineral admixtures to modify the properties and lower the raw material costs of BMS. Zhang et al. [13] studied the effects of high and low calcium fly ash on the basic properties, microstructure, and water resistance of BMS. The results showed that both types of fly ash could improve the compressive strength and softening coefficient of BMS. Tan et al. [14] investigated the effect of silica fume (SF) on the properties and hydration mechanism of BMS. The results showed that the filling effect of SF led to a more compact microstructure of the matrix, which increased the compressive strength of the BMS. Moreover, SF was activated in the BMS matrix, leading to the formation of M-S-H gels.

In addition to the effect of the admixture, the active $MgO/MgSO_4$ molar ratio (MSMR) was found to affect the properties of BMS. Wu [19, 20] investigated the effect of MSMR on the compressive strength and phase composition of BMS, Huang et al. [17] used the thermodynamic database to study the dependence of the equilibrium phase composition on the molar ratio as well. The above results showed that when MSMR was 3, the main crystalline phase contributing to the strength was $3Mg(OH)_2$-$MgSO_4$-$8H_2O$ (3-1-8). When the MSMR increased to 5, 3-1-8 gradually disappeared and a new magnesium sulfate phase precipitated, which is expressed as $5Mg(OH)_2$-$MgSO_4$-$7H_2O$ (5-1-7), at which point the compressive strength of BMS increased significantly. When the MSMR was in a range from 7 to 8, the mass fraction of SO_4^{2-} and Mg^{2+} in the gelling system decreased, which could cause the nucleation of $Mg(OH)_2$ and the appearance of new exothermic hydration peaks during the hydration of BMS, leading to the reverse shrinkage of the compressive strength.

Steel slag (SS) is a by-product of the steel industry, the mineral composition of which is mainly calcium silicate. In China, steel slag has become one of the most important sources of industrial waste, with less than 20 % of SS currently being utilised [18]. The waste steel slag occupies a large area of land and leads to many serious environmental problems, so the reuse of SS has also garnered increasing attention. Huang et al. [19] studied the effect of SS addition on the hydration characteristics and compressive strength of BMS. The results showed that although the addition of SS would reduce the 5-1-7 content in BMS and lead to a decrease in the mechanical properties, SS additions below 10 % could meet an acceptable degree of mechanical properties.

Previous studies showed that the MSMR significantly affects the mechanical properties and hydration production of BMS. For BMS with the incorporation of SS (BMS-SS), an appropriate MSMR is pivotal to attain good mechanical performance, which can promote the application of SS in magnesium-based cements. Thus, in this work, the effect of MSMR on the mechanical properties of BMS-SS was investigated. The mechanism of the influence was analysed in view of the exothermic hydration performance, the composition of the hydration product, the microscopic morphology, and the pore structure.

EXPERIMENTAL

Raw materials

Light-burned magnesia (LBM) and an analytical grade $MgSO_4 \cdot 7H_2O$ reagent were used in the study to prepare the BMS, and analytical grade $C_6H_8O_7$ was added as the chemical admixture. The activity index of LBM is 66.24 %, tested by the standard hydration method [19]. The chemical compositions of LBM and SS used in the study were determined by X-ray fluorescence analysis and are shown in Table 1.

Table 1. Chemical composition (%).

	MgO	SiO_2	Fe_2O_3	CaO	Al_2O_3	K_2O	Na_2O	SO_3	MnO
LBM	83.10	6.12	3.01	5.93	0.79	0.07	–	0.23	0.21
SS	11.05	20.06	16.24	41.76	8.78	0.52	0.43	1.16	–

Sample Preparation

Three MSMRs were selected for this experiment, 5, 7 and 9. The molar ratio of $H_2O/MgSO_4$ is 20:1, the mass fraction of the $MgSO_4$ solution is 25.0 %, the substitution degree of the SS is 10 % of the mass of the LBM, and the additional amount of citric acid is 0.5 % of the mass of the LBM. In order to distinguish the influence of the SS, the BMS samples without SS were prepared as the control groups, noted as M5, M7 and M9, respectively. In contrast, the samples M5S, M7S and M9S are the experimental groups with the 10 % SS addition. The mix proportions are shown in Table 2.

Table 2. Mix proportions (g).

Samples	MgO	$MgSO_4 \cdot 7H_2O$	H_2O	Steel slag	Citric acid
M5	200	317.9	0	0	1
M5S	180	286.2	15.5	36.3	0.9
M7	200	227.1	0	0	1
M7S	180	204.3	11.0	31.6	0.9
M9	200	176.6	0	0	1
M9S	180	159.1	8.6	29.1	0.9

First of all, according to mix proportions in Table 2, the ingredients of each samples were weighed accurately. Then, $MgSO_4 \cdot 7H_2O$ was added to deionised water and the mixture was continuously stirred to prepare a 25 % mass fraction of the magnesium sulfate solution. Afterwards, the weighed LBM, SS (no SS was added to the control group), and the citric acid ingredients were added in turn and mixed. The mixed cement paste was injected into a 20 mm × 20 mm × 20 mm stainless steel mould, then cured at (20 ± 2) °C with a relative humidity of 95 %. After 1 d of curing, the mould was removed and the curing continued until the intended test age for testing.

Test method

A 4-channel isothermal calorimeter (Calmetrix-4000HPC) was used to monitor the heat release of BMS and BMS-SS with the different MSMRs, which was conducted at 20 °C and lasted for 72 h. When the prepared BMS and BMS-SS specimens reached the test ages (1, 3, 7 and 28 d), the compressive strength was tested using a TYE-300F mortar flexure and compression tester with a maximum pressure of 300 kN, according to the GB/175-2007 standard. The crushed pieces were tested for the pore size distribution using an automatic mercury porosimeter (AutoPore IV 9500, Micromeritics, Norcross, Georgia, USA). The remainder was ground in an agate mortar with an appropriate amount of anhydrous ethanol until it all passed through an 80 μm square pore sieve, and then the test was carried out using an X-ray diffractometer (D/max-2500pc, RIGAKU, Tokyo, Japan) with an accelerating voltage of 30 kV and a 2θ range of 5° – 65° in steps of 0.02°. Rietveld full spectrum fitting was conducted for the quantitative analysis using Jade 6.5. A thermal gravimetric analyser (HCT-1, HENVE, Beijing, China) was used to determine the thermal properties of the samples at a heating rate of 10 °C min^{-1} and the samples were heated from 30 °C to 1050 °C.

RESULTS AND DISCUSSION

Hydration process

The hydration characteristics of the BMS before 72 h are clearly shown in Figure 1. As shown in Figure 1a, the length of induction period changes with the MSMR, while M7 has the shortest induction period, the induction period of M9 is the longest. With an increase in the MSMR, the induction period of BMS shortens first, then extends. The trend is in line with the change in the time that the main exothermic peak appears. Moreover, the intensity of the main exothermic peak is influenced by the MSMR. The peak intensities of M5, M7 and M9 are 1.83 mW·g^{-1}, 2.08 mW·g^{-1} and 2.02 mW·g^{-1}, respectively. It should also be noted that the decrease of M9 exothermic rate is extremely fast; an inflection point appears at about 45 h. As shown in Figure 1b, the cumulative heat of M7 at 72 h is the highest among the samples, and the cumulative heat of M5 and M9 is less than M7 by 15.46 J·g^{-1} and 2.91 J·g^{-1}, respectively.

The main exothermic peak is the heat release of the formation of 5-1-7 [14], the duration of the induction period is dependent on the time required for the nucleation of 5-1-7. The content of Mg^{2+}, SO_4^{2-} and OH- in the liquid phase is critical. The shortest induction period of M7 indicates the composition of its liquid phase is most favourable for the nucleation of 5-1-7. Compared to that of M5 and M7, the magnesium in M9 is far more than surplus, the excessive Mg^{2+} lead to the formation of $Mg(OH)_2$, which accounts for the exothermic peak after the inflection point in the exothermic peak curve.

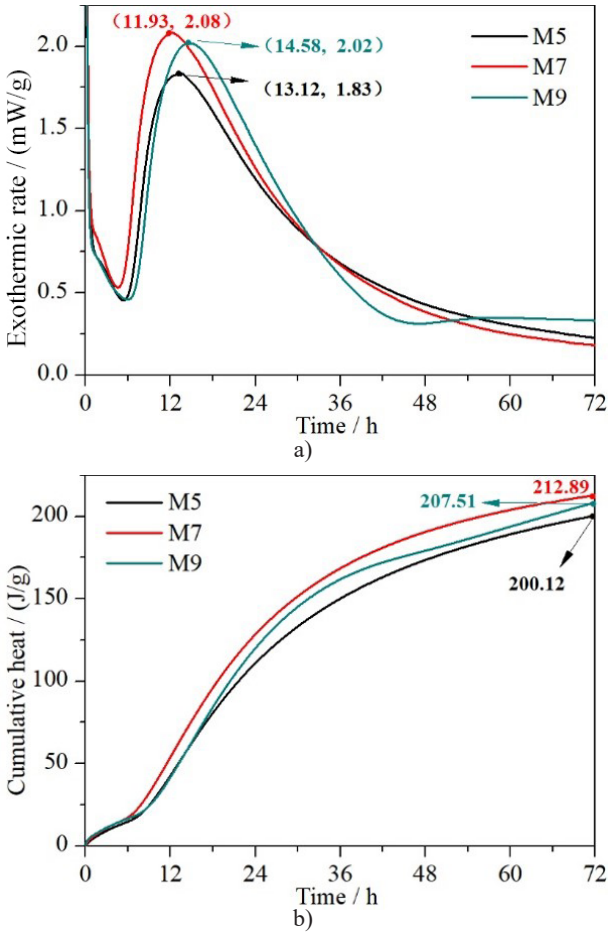

Figure 1. Exothermic rate and cumulative heat release of the BMS.

The incorporation of SS leads to an extension in the induction period and a decline in the intensity of the main exothermic peak. However, the differences in the length of the induction period led by the MSMR are weakened by the SS addition. As shown in Figure 2a, the differences between the times corresponding to the main exothermic peaks are less than 0.4 h for the samples with the different MSMRs. The intensities of the main exothermic peaks for M5 and M9 are almost the same. The cumulative heat of BMS is decreased by the SS addition, the SS-incorporated sample with an MSMR of 7 has the highest cumulative heat release.

The incorporation of SS leads to a relative decrease in the MgO content, the total contents of Mg^{2+}, SO_4^{2-} dissolved into the liquid phase consequently decrease, which is not conducive to the nucleation of 5-1-7. Thus, the induction periods of the samples with SS addition are shortened, and the intensities are significantly weakened. As mentioned above, the difference

in the exothermic rate of BMS with the different MSMRs results from the different liquid compositions of the samples, the decrease in the total content of reactant ions diminishes the difference. Moreover, the content of citric acid added is based on the content of MgO. For BMS-SS, a portion of the citric acid is inevitably consumed by the SS reaction, which is also negative for the formation of 5-1-7. Thus, the difference in the curves of BMS-SS with the different MSMRs is negligible.

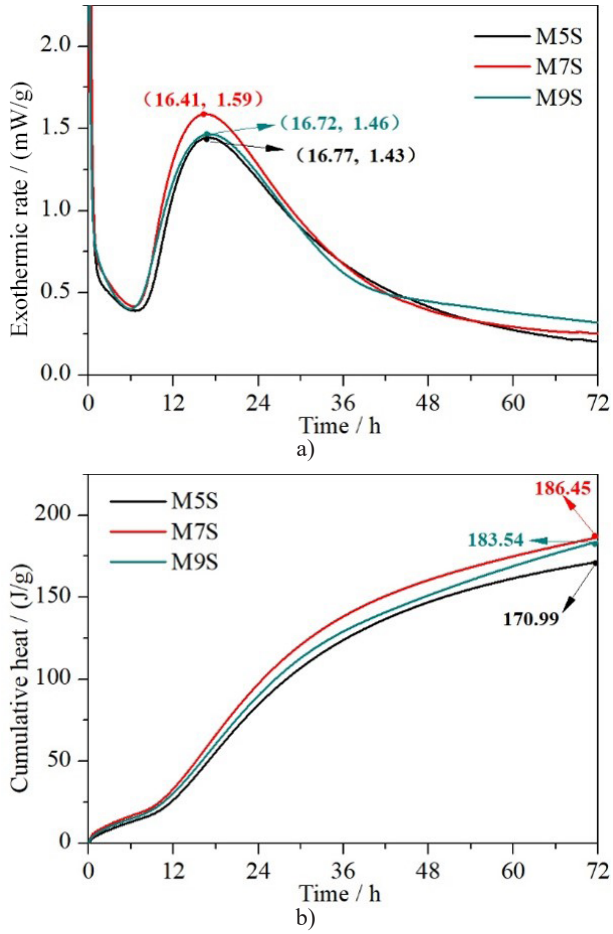

Figure 2. Exothermic rate and cumulative heat release of BMS-SS.

TG analysis

Figures 3 and 4 show the mass change of the samples with the increase in the temperature at 3 d and 28 d. It can be seen that there are 6 peaks in the DTG curves. P1, P2 and P4 result from the thermal decomposition of 5-1-7 (the loss of the chemically bond water). At 3 d, the intensity of these peaks for M5 is stronger than M7 and M9, meaning that a low MSMR can promote the formation of 5-1-7 phase in the early age. As shown in Figure 4a, MSMR has the same effects on the samples with the SS incorporation. With an increase in the curing age, the intensity of these peaks shows no significant difference for the BMS, indicating that more of 5-1-7 phase forms in the samples with a high MSMR in the later age. For the samples with the SS incorporation, there is still a prominent difference in the intensity of the peaks, the SS incorporation suppresses the formation of 5-1-7 in the samples with a high MSMR in the late age.

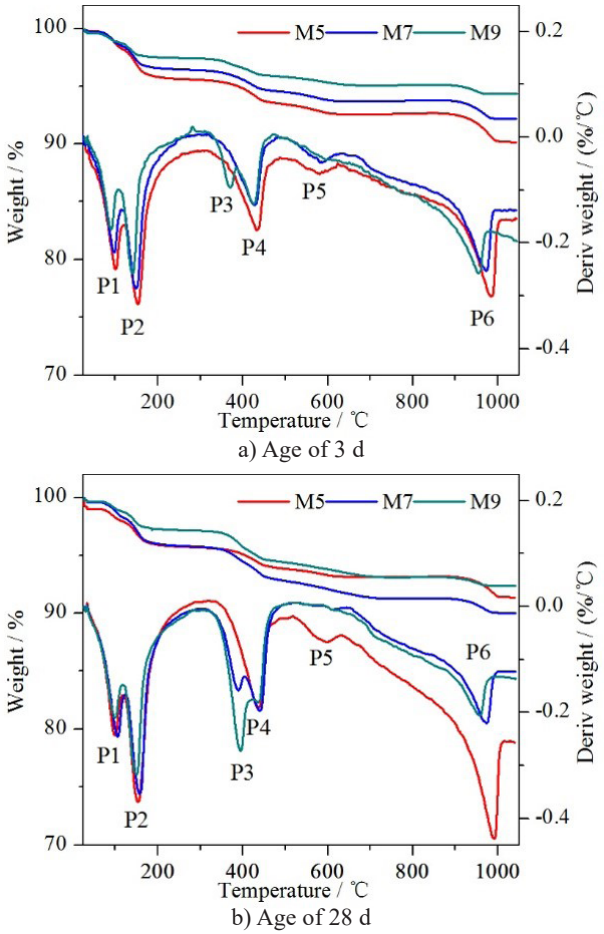

Figure 3. TG and DTG curves of the BMS samples.

In addition to the peaks corresponding to the thermal decomposition of 5-1-7, another three peaks should be noted. P3 results from the thermal decomposition of $Mg(OH)_2$, P5 represents the thermal decomposition of $MgCO_3$, and P6 denotes the thermal decomposition of $MgSO_4$. The chemical reaction formulas are shown as Equation 1 and 2. The mass fractions of $Mg(OH)_2$ and $MgSO_4$ can be calculated and are shown in Table 3 and Table 4.

$$Mg(OH)_2(s) \xrightarrow{360\ ^\circ C} MgO(s) + H_2O \quad (1)$$

$$MgSO_4(s) \xrightarrow{950\ ^\circ C} MgO(s) + SO_3 \quad (2)$$

At 3 d, $Mg(OH)_2$ only forms in M9, which has the highest MSMR among the samples. A high MSMR facilitates the formation of $Mg(OH)_2$. The incorporation of SS leads to the formation of $Mg(OH)_2$ even

Table 3. Mass fraction of $Mg(OH)_2$ (%).

Age	M5	M7	M9	M5S	M7S	M9S
3 d	0	0	1.93	0.81	0.67	1.67
28 d	0	4.32	6.09	1.93	1.61	2.19

Table 4. Mass fraction of $MgSO_4$ (%).

Age	M5	M7	M9	M5S	M7S	M9S
3 d	4.72	3.20	1.52	1.86	1.28	0.66
28 d	3.54	2.50	1.60	1.00	1.48	0.64

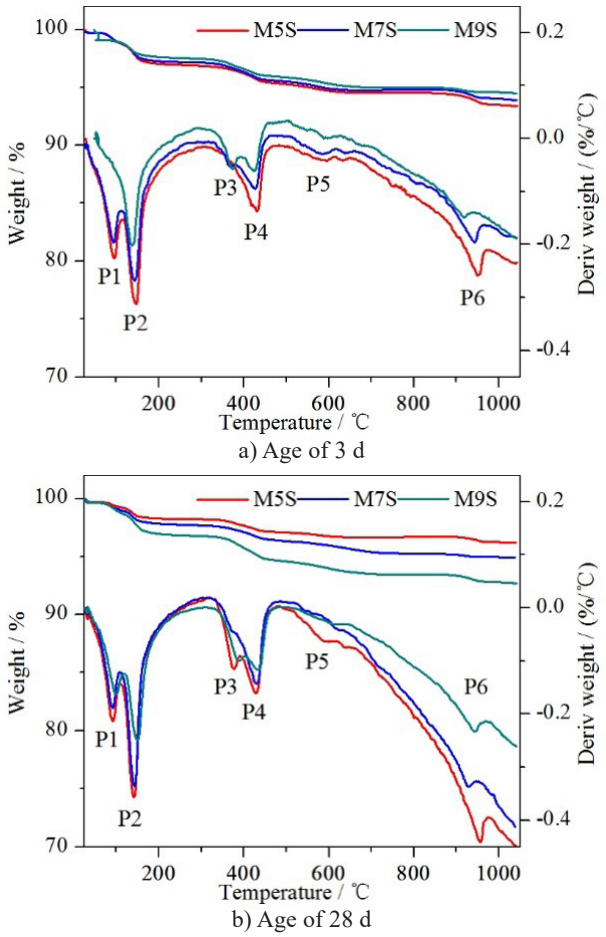

Figure 4. TG and DTG curves of the BMS-SS samples.

for the sample with a low MSMR. Compared to M9, the $Mg(OH)_2$ formed in M9S is less by 0.26 %. When the age comes to 28 d, there is still no $Mg(OH)_2$ formed in M5. The mass fractions of $Mg(OH)_2$ formed in M7 and M9 are 4.32 % and 6.09 %, respectively. The increase is due to the continuous hydration of MgO. Identical to the BMS samples, the content of $Mg(OH)_2$ formed in the samples with the SS incorporation increases with the age. However, the increase range of the $Mg(OH)_2$ content in BMS-SS is less than that of BMS. The mass fraction of $MgSO_4$ shown in Table 4 is in line with the variation of the MSMR; the lower the magnesium/sulfur of the sample is, the more the $MgSO_4$ exists. With an increase in the age, the $MgSO_4$ decreases through the continuous hydration of the samples. The incorporation of SS decreases the content of $MgSO_4$, which could be due to some new reaction caused by the SS incorporation.

XRD analysis

The diffraction patterns of the samples at 3 d and 28 d are shown in Figure 5. The diffraction peaks of the hydrates and reactants, which have already been identified in the TG analysis, are all shown in the patterns, including the 5-1-7 phase, $Mg(OH)_2$, $MgCO_3$ and MgO. In addition, there are noteworthy diffraction peaks of gypsum ($CaSO_4 \cdot 2H_2O$) in the patterns of the samples with the SS incorporation at both 3 d and 28 d. At 3 d, the diffraction peaks of gypsum for M5S are the highest among the samples with the SS incorporation. Compared to M7S and M9S, the content of sulfur existing in M5S is the highest, which favours the formation of gypsum. However, when the age comes to 28 d, the diffraction peaks of gypsum for M7S and M7S are significantly enhanced, as shown in Figure 5b.

The mass fractions of 5-1-7 obtained through the quantitative XRD method are shown in Table 5. The mass fractions of 5-1-7 in the samples with an MSMR of 5 and 7 are almost equal, whether or not SS is incorporated. For the samples with an MSMR of 9, the mass fraction of 5-1-7 is far less than the other two ratios. Thus, it can be remarked that the sulfate content in the sample of BMS with an MSMR of 7 is adequate for the formation of 5-1-7. The excess sulfate content in the BMS or BMS-SS when the MSMR is less than 7 has no significant promoting effect on the formation of 5-1-7. For the samples with the SS incorporation, an MSMR of 7 is still the key point for the formation of 5-1-7.

Table 5. Mass fraction of 5-1-7.

Age	M5	M7	M9	M5S	M7S	M9S
3 d	54.9	54.6	49.2	52.5	52.3	35.3
28 d	63.7	62.3	44.6	53.6	51.7	32.1

At 3 d, for the samples with an MSMR of 5 and 7, the incorporations of SS did not dramatically decrease the formation of 5-1-7. Whereas, for the sample with an MSMR of 9, the formation of 5-1-7 is significantly decreased by the SS incorporation. Compared to M9, the sulfates in M5 and M7 are abundant. As shown in Figure 5, the SS incorporation leads to the formation of gypsum, SO_4^{2-} is consumed in the process. For M5 and M7, the decrease in SO_4^{2-} content does not significantly affect the formation of 5-1-7. Whereas for M9, which has a low sulfate content, the decrease leads to an insufficiency of SO_4^{2-} for the formation of 5-1-7 and, therefore, causes a significant decrease in the

content of 5-1-7. The excess magnesium in M9S hydrates and forms more $Mg(OH)_2$, as shown in Table 3.

With an increase in the age, the content of 5-1-7 in the samples of M5 and M7 has a noticeable increase, and the content in M9 decreases. As introduced in Raw materials section, the LBM used in the study is composed of MgO with different activities. Highly active MgO hydrates at an early age; a period of time is required for the dissolution of low-active MgO, which could provide Mg^{2+} at a late age. Thus, there is a remarkable increase in the content of 5-1-7 for M5 and M7, which are rich in SO_4^{2-}. Though Mg^{2+} in M9 is continuously supplied, there is not a noticeable increase in the content of 5-1-7 due to the lack of SO_4^{2-} content. For all the samples with the SS incorporation, the content of 5-1-7 is almost unchanged with the increase in age. The lack of the SO_4^{2-} content, led by the consumption of the gypsum formation, accounts for the unchanged content of 5-1-7. Based on the above, a conclusion can be drawn that the continuous formation of 5-1-7 depends on the sulfate content: a higher sulfate content could support the constant formation of this phase in the BMS and BMS-SS.

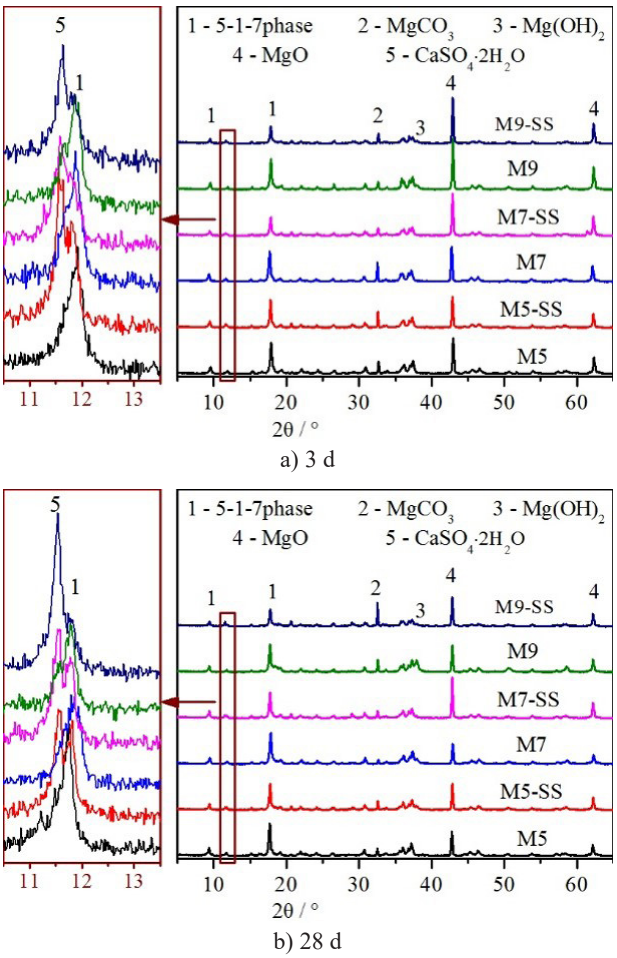

Figure 5. XRD patterns of the BMS and BMS-SS samples.

Pore structures

Figure 6 shows the cumulative pore volume and incremental pore volume of BMS at 28 d. The porosity of M5 is 0.39, whereas those of M7 and M9 are 0.28 and 0.26, respectively. Moreover, the aperture distribution is also different with the va-riation in the MSMR. As shown in Table 6, the average pore diameter of M7 is the lowest, the proportions of pores less than 20 nm in M7 and between 20 – 100 nm are higher than that in M5 and M9. Pores larger than 100 nm are formed the most in M9.

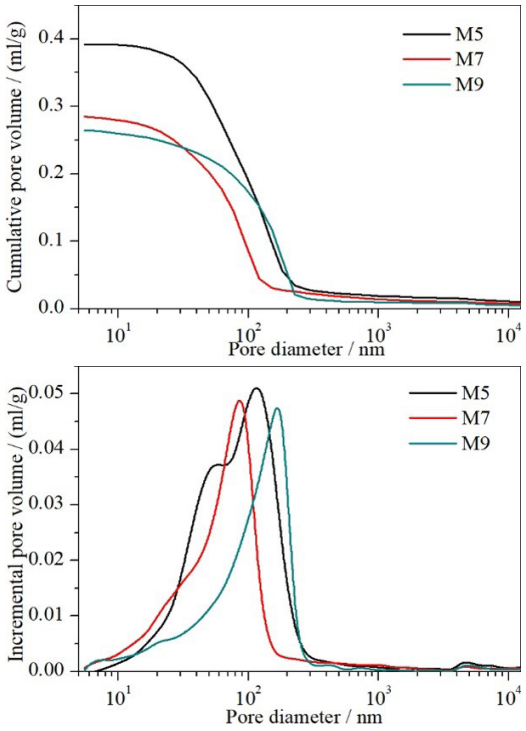

Figure 6. Pore structures of the BMS samples at 28 d.

During the sample preparation, the mass of MgO is referred to as the reactive MgO in the LBM, so the different MSMRs of the samples lead to different water-to-binder ratios. For a sample with a higher MSMR, more inactive MgO, which is not included in the mass of MgO, is introduced into the sample. Thus, the higher the MSMR, the lower the practical water-to-binder ratio. The highest porosity of M5 is attributed to its highest practical need for the water-to-binder ratio. There is not a significant difference in the porosity between M7 and M9, though the practical water-to-binder ratio of M7 is far greater than that of M9. It is due to the higher content of 5-1-7, which could fill the pores previously occupied by the water in M7, compared to that in M9.

The cumulative pore volume and incremental pore volume of BMS-SS are shown in Figure 7. The porosity of M5S, M7S, and M9S is 0.37, 0.275, and 0.32, respectively. Compared to the BMS samples

with the same MSMR, the incorporation of SS leads to an increase in the porosity for the samples with the MSMR of 9, and slightly decreases for the samples with the MSMR of 5 and 7. The effect of the SS incorporation on the porosity of the sample with the MSMR of 7 is the least accentuated.

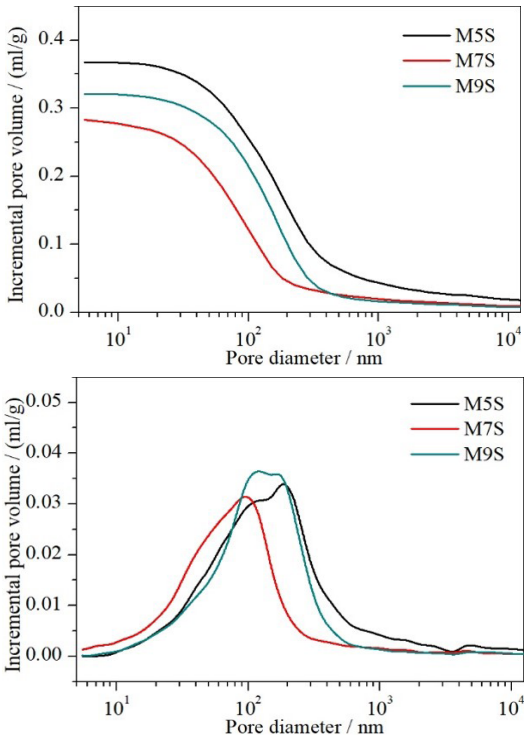

Figure 7. Pore structures of the BMS-SS incorporations at 28 d.

The SS incorporations lead to the formation of gypsum and the slowing down of the formation of 5-1-7 and $Mg(OH)_2$ for the samples with the same MSMR. Based on TG and XRD analysis, the content of gypsum and $Mg(OH)_2$ formed in M9S is higher than that of M5S and M7S. Gypsum is a kind of large-size tabular crystal that can induce the cracking failure of concrete [20]. $Mg(OH)_2$ is a kind of hexagonal sheet crystal that can induce the expansion of concrete and be applied as an expansion agent in concrete engineering [21]. Both the growth of gypsum and $Mg(OH)_2$ can fill the pores in hardened pastes, but the excessive growth will break them apart. As mentioned before, the practical need for a water-to-binder ratio of M9 is lower than M5 and M7, which results in a lower porosity. The expansion and cracking, induced by the growth of gypsum and $Mg(OH)_2$, are more likely to occur for the pastes with a lower porosity. Thus, the increase in porosity of M9S could be attributed to the growth of gypsum and $Mg(OH)_2$.

As shown in Table 6, among the samples with the SS incorporation; the average pore diameter of M7S is still the lowest; the average pore diameters of the other two samples are larger by 51.01 nm and 37.09 nm compared to M7S. The SS incorporations enlarge the average pore diameter for all the samples. Because the content of formed 5-1-7 decreases with the addition of SS, large pores cannot be filled as well in the BMS samples. In addition, pores less than 20 nm, for all the samples, decrease with the SS incorporation. Our previous study found that C-S-H formed in BMS pastes with an SS incorporation [19]. Pores less than 20 nm, which cannot be filled with 5-1-7, can be easily filled with the gel products – C-S-H.

Table 6. Classification statistics of the pore structures at 28 d.

Samples	Average pore diameter (nm)	< 20 nm (%)	20–100 nm (%)	> 100 nm (%)
M5	71.57	2.83	58.32	38.85
M7	49.94	7.89	76.48	15.63
M9	69.70	5.82	36.64	57.54
M5S	105.49	1.89	34.99	63.12
M7S	54.48	7.08	59.05	33.87
M9S	91.57	2.56	39.01	58.43

Based the on the above analysis, it can be concluded that 7 is the optimal ratio of the MSMR (compared to 5 and 9). A higher MSMR would lead to a lack of sulfate in the reaction system and, therefore, they suppress the formation of 5-1-7. The sulfate content in the specimen with an MSMR of 7 is sufficient for the formation of 5-1-7, a lower MSMR cannot lead to a significant increase in the formation of 5-1-7, but it can lead to an increase in the water-to-binder ratio, consequently, the porosity is greatly enlarged.

Mechanical properties

The compressive strength of the samples with the different MSMRs are shown in Figure 8. There is not a significant difference in the compressive strength between M7 and M9. The compressive strength of M5 in all the tested ages is prominently lower than that of M7 and M9. These are in line with the variations in the porosities shown in Figure 6. The lower the porosity, the higher the compressive strength. The incorporation of SS decreases the compressive strength for all the samples. The compressive strength of M5S is still the lowest. Besides, there is a prominent gap in the compressive strength between M7S and M9S. The growth of gypsum and $Mg(OH)_2$ has a negative effect on the development of the compressive strength of M9S.

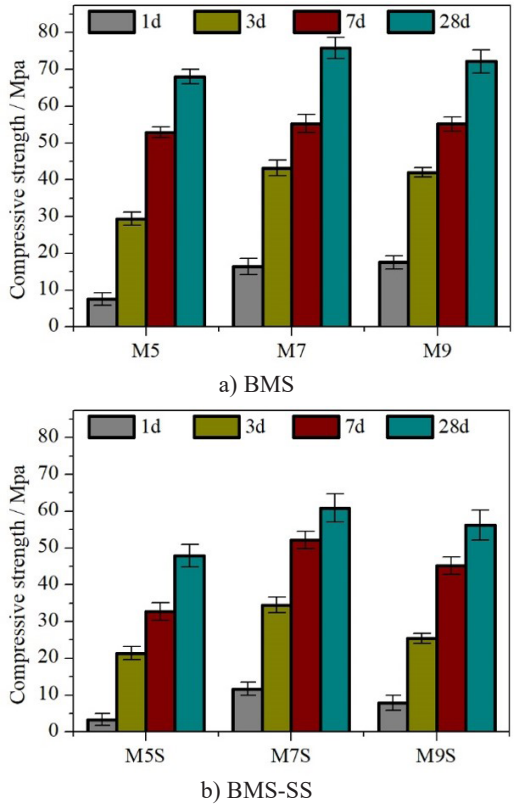

Figure 8. Compressive strength.

CONCLUSIONS

The following conclusions can be drawn based on the above results and discussion.

(1) The hydration process of BMS and BMS-SS are both affected by the MSMRs; samples with an MSMR of 7 have the highest cumulative heat both for BMS and BMS-SS.

(2) A higher MSMR negatively affects the formation of the 5-1-7 phase, but supports that of $Mg(OH)_2$. Moreover, the incorporation of SS leads to the formation of gypsum, especially for the samples with a low MSMR.

(3) The porosity and pore size distribution are affected by the MSMRs, the porosity of the samples with an MSMR of 5 are significantly higher than that of 7 and 9, and the average pore diameter of the samples with an MSMR of 7 is the lowest whether or not SS is incorporated.

(4) The compressive strength of the samples with an MSMR of 7 and 9 are nearly equal and prominently higher than those with an MSMR of 5. However, the SS incorporations lead to a decrease in the compressive strength for all the samples.

The effect of the MSMR on the microstructure and mechanical properties of BMS and BMS-SS show the same tendency. An MSMR of 7 is the optimal ratio (compared to 5 and 9 in the study) for BMS-SS to acquire a compact microstructure and favourable mechanical properties.

Acknowledgments

The authors would like to acknowledge the financial support of Qinghai Provincial Science and Technology Department Basic Research Project (2022-ZJ-980Q), and Qinghai Provincial Key Laboratory of Plateau Green Building and Eco-community Open Fund Project (KLKF-2021-002).

REFERENCES

1. Walling S. A., Provis J. L. (2016): Magnesia-based cements: a journey of 150 years, and cements for the future? *Chemical reviews, 116*(7), 4170-4204. doi: 10.1021/acs.chemrev.5b00463
2. Gomes C. M., de Oliveira A. D. S. (2018): Chemical phases and microstructural analysis of pastes based on magnesia cement. *Construction and Building Materials, 188*, 615-620. doi: 10.1016/j.conbuildmat.2018.08.083
3. Zeng X., Yu H., Wu C. (2019): An overview of study on basic magnesium sulfate cement and concrete in China (2012–2019). KSCE *Journal of Civil Engineering, 23*(10), 4445-4453. doi: 10.1007/s12205-019-0199-7
4. Wu C., Chen W., Zhang H., Yu H., Zhang W., Jiang N., Liu L. (2017): The hydration mechanism and performance of Modified magnesium oxysulfate cement by tartaric acid. *Construction and Building Materials, 144*, 516-524. doi: 10.1016/j.conbuildmat.2017.03.222
5. Runčevski T., Wu C., Yu H., Yang B., Dinnebier R. E. (2013): Structural characterization of a new magnesium oxysulfate hydrate cement phase and its surface reactions with atmospheric carbon dioxide. *Journal of the American ceramic society, 96*(11), 3609-3616. doi: 10.1111/jace.12556
6. Tan Y., Wu C., Yu H., Li Y., Wen J. (2021): Review of reactive magnesia-based cementitious materials: Current developments and potential applicability. *Journal of Building Engineering, 40*, 102342. doi: 10.1016/j.jobe.2021.102342
7. Gong W., Yu H., Ma H., Wang N., He L. (2020): Study on the basic performance of basic magnesium sulfate cement concrete. *Emerging Materials Research, 9*(3), 618-627. doi: 10.1680/jemmr.19.00039
8. Wu C., Yu H., Zhang H., Dong J., Wen J., Tan Y. (2015): Effects of phosphoric acid and phosphates on magnesium oxysulfate cement. *Materials and Structures, 48*(4), 907-917. doi: 10.1617/s11527-013-0202-6
9. Wang, N., Yu, H., Bi, W., Guan, Y., Gong, W., Zhang, N., & Wu, C. (2021): The Improvement Effects of NaH2PO4 and KH2PO4 on the Properties of Magnesium Oxysulfate Cement. *Journal of Wuhan University of Technology-Mater. Sci. Ed., 36*(1), 50-57. doi: 10.1007/s11595-021-2377-y
10. Wang N., Yu H., Bi W., Tan Y., Zhang N., Wu C., Hua S. (2018): Effects of sodium citrate and citric acid on the properties of magnesium oxysulfate cement. *Construction and Building Materials, 169*, 697-704. doi: 10.1016/j.conbuildmat.2018.02.208
11. Tan Y., Yu H., Yang D., Feng T. (2022): Basic magnesium sulfate cement: Autogenous shrinkage evolution and mechanism under various chemical admixtures. *Cement and Concrete Composites, 128*, 104412. doi: 10.1016/j.

cemconcomp.2022.104412
12. Guo T., Wang H., Yang H., Cai X., Ma Q., Yang S. (2017): The mechanical properties of magnesium oxysulfate cement enhanced with 517 phase magnesium oxysulfate whiskers. *Construction and Building Materials, 150*, 844-850. doi: 10.1016/j.conbuildmat.2017.06.024
13. Zhang N., Yu H., Gong W., Liu T., Wang N., Tan Y., Wu C. (2020): Effects of low-and high-calcium fly ash on the water resistance of magnesium oxysulfate cement. *Construction and Building Materials, 230*, 116951. doi: 10.1016/j.conbuildmat.2019.116951
14. Tan Y., Yu H., Sun S., Wu C., Ding H. (2021): Properties and microstructure of basic magnesium sulfate cement: Influence of silica fume. *Construction and Building Materials, 266*, 121076. doi: 10.1016/j.conbuildmat.2020.121076
15. Wu C., Miao M., Yu H. (2021): Effect of MgO Activity and Molar Ratio on Strength of Basic Magnesium Sulfate Cement and Its Mechanism. *Journal of Building Materials, (04)*, 360-366. (In Chinese) doi:10.3969/j.issn.1007-9629.2022.04.005
16. Wu C., Yu H., Dong J., Zheng L. (2014): Effects of material ration, fly ash, and citric acid on magnesium oxysulfate cement. *ACI Materials Journal, 111*(3), 291. doi: 10.14359/51686723
17. Huang J., Li W., Huang D., Wang L., Chen E., Wu C. et al. (2021): Fractal analysis on pore structure and hydration of magnesium oxysulfate cements by first principle, thermodynamic and microstructure-based methods. *Fractal and Fractional, 5*(4), 164. doi: 10.3390/fractalfract5040164
18. Hu Z., Guan Y., Chang J., Bi W., Zhang T. (2020): Effect of Carbonation on the Water Resistance of Steel Slag—Magnesium Oxysulfate (MOS) Cement Blends. *Materials, 13*(21), 5006. doi: 10.3390/ma13215006
19. Huang Z., Huang L., He X. (2022): Hydration Characteristics and Mechanic Properties of Basic Magnesium Sulfate Cement Containing Steel Slag. *Journal of Advanced Concrete Technology, 20*(4), 277-286. doi:10.3151/jact.20.277
20. Huang L., Yan P. (2019): Effect of alkali content in cement on its hydration kinetics and mechanical properties. *Construction and Building Materials, 228*, 116833. doi: 10.1016/j.conbuildmat.2019.116833
21. Cao F., Liu Y., Yan P. (2021): Properties and mechanism of the compound MgO expansive agent (CMEA) produced by calcining the mixture of dolomite and serpentine tailings. *Construction and Building Materials, 277*, 122331. doi: 10.1016/j.conbuildmat.2021.122331